Non peer-reviewed preprint uploaded to Engrxiv

Validation of seismic performance of an advanced sand constitutive model on experimental work on soil-structure interaction

Piotr Kowalczyk
Independent Researcher
formerly Department of Civil, Environmental and Mechanical Engineering, University of Trento
Via Mesiano 77, 38123 Trento (Italy)
Email address of the corresponding author: pk.piotrkowalczyk.pk@gmail.com
ORCID number: 0000-0003-0777-6429

Abstract:

There is a growing number of available advanced soil constitutive models aimed at capturing soil cyclic behaviour and their subsequent use in seismic and offshore applications. Nevertheless, detailed validation studies of these soil constitutive models on benchmark experimental works on offshore or seismic soil-structure interaction are still rare. This work presents validation of seismic performance of an advanced elastoplastic sand constitutive model on a large boundary value problem of soil-structure interaction studied previously experimentally. The elastoplastic constitutive model is innovative in a way of using a hyperelastic law inside the yield surface. The finite element numerical results are compared with the experimental work on a group of piles analysed in a flexible soil container filled with dry sand and subjected to simplified seismic loading. In general, the comparisons show a satisfactory match between the results of the simulations and the experiments and confirm the suitability of the investigated soil constitutive model to carry out predictive seismic geotechnical analysis in the future.

Keywords: finite element modelling, soil constitutive modelling, soil-structure interaction, soil dynamics, high frequencies.

1. Introduction

Soil behaviour and soil-structure interaction (SSI) under seismic and offshore loading conditions have been widely studied in recent years. Comprehensive understanding of SSI is of paramount importance for resilient cities of the future. The origin of SSI comes from the fact that soil causes a structure to vibrate, and the vibrating structure in response affects the surrounding soil. The SSI can be split into kinematic interaction (when an embedded structure has stiffness but no mass and the behaviour of the structure tends to be driven by soil seismic waves) and inertial interaction (when the embedded structure has also mass which affects the motion of the surrounding soil). Typically, when compared to the fixed base conditions, SSI leads to lengthening of natural periods and increased damping due to wave radiation effect and hysteretic damping due to plasticity developing in soil (Pitilakis et al. [1]). A similar point of view to soil-structure interaction was presented by Loli et al. [2] where the authors indicated soil as a potential placement of a plastic hinge developing during large magnitude earthquakes in a system and, therefore, protecting structures. Although typically soil influence on structures is considered beneficial, detrimental effects can also be observed. An example of that is the 1985 Mexico City Earthquake, where double resonance was experienced, i.e. soil vibrated with its own natural frequency, and then caused structures of similar natural frequency to resonate with the soil natural frequency which as a result suffered substantial damage (Hall & Back [3]). Indeed, Mylonakis & Gazetas [4] looked in detail at cases of detrimental effects of SSI and concluded that structural ductility demand can also increase due to period elongation caused by SSI. Although generally the SSI effects have been acknowledged, further advanced experimental and numerical studies follow in order to detail the knowledge on SSI and allow improved predictions of the response of real structures to earthquakes.

Small scale physical modelling is one of the approaches to study the dynamic behaviour of soil and SSI under earthquake conditions and, subsequently, to allow validation of numerical studies. Numerous experimental studies have been carried out in the recent past. Many of them have been carried out on dry sand in shear stacks on a shaking table in 1-g stress state (Muir Wood et al. [5]). For example, Massimino & Maugeri [6] analysed two structures resting on shallow foundations to investigate soil-foundation interaction. Chidichimo et al. [7] studied a pile group behaviour in a bi-layered soil profile. Further comments and outcomes of the latter experimental work were also shown by Simonelli et al. [8] and Durante et al. [9]. Another group of physical studies on seismic soil-structure interaction comprises those carried out in centrifuge, thus at the increased stress levels comparing to 1-g stress state conditions. For example, Lanzano et al. [10] studied a tunnel embedded in granular dry soil subjected to earthquake loading with the final aim to allow future validation of numerical tools. Conti et al. [11] looked at the behaviour of a retaining wall, its rotation and distribution of earth pressures in dry sand under seismic loading. Many centrifuge studies have been carried out on saturated sand. A case of a saturated slope in a rigid box which had been studied within the LEAP-GWU-2015 and LEAP-UCD-2017 projects was later summarized by Kutter et al. [12] and Kutter et al. [13] respectively, where the results from all the participating centrifuge centres were compared. In addition to small scale experimental tests, there is a lower number of large-scale experimental works on seismic SSI. For instance, Tokimatsu et al. [14] studied kinematic and inertial interaction of a small pile group with and without a structure in dry and saturated soil. Shirato et al. [15] showed subsequently a larger pile group subjected to a series of large-scale earthquakes.

Numerical modelling, such as the finite element method, is a powerful tool to study seismic soil behaviour and SSI, and is an attractive alternative to physical modelling. Robust advanced soil constitutive models capable of simulating cyclic soil behaviour are needed to carry out reliable predictions in numerical studies. There is a vast number of advanced sand constitutive models which come from different theoretical frameworks and which have been shown to be able to replicate soil cyclic behaviour, thus they were indicated to be good candidates to be used in seismic analysis in large boundary value problems. For instance, Gajo & Muir Wood [16][17] presented a kinematic hardening elastoplastic model, namely the Severn-Trent sand model, which was shown to be capable of replicating sand cyclic behaviour in single element laboratory tests under various densities and pressures with a single set of model parameters.

A group of soil constitutive models also building on elastoplasticity theory and capable of simulating soil cyclic behaviour comes under the name of SANISAND (simple anisotropic sand) family models. These models include consecutive works from Dafalias & Manzari [18], Dafalias et al. [19], Taiebat & Dafalias [20], Dafalias & Taiebat [21] which are all based on Manzari & Dafalias [22] and introduced, respectively, the following updates: a fabric tensor to modify volumetric response, a fabric tensor to account for inherent anisotropy, a yield cup to model grain crushing, and a model without a yield surface. The SANISAND family models were also bases and inspirations for further developments by other researchers. For example, Pisano & Jeremic [23] proposed a visco-elastic-plastic constitutive model which poses two dissipative mechanisms, first due to hysteric soil behaviour, second due to viscous damping. A popular choice among practitioners dealing with liquefaction phenomena in saturated soil is the PM4 sand model (Boulanger & Ziotopoulou [24]) which was also based on the basic structure of the SANISAND models.

A different family of soil constitutive models successfully dealing with soil cyclic loading is based on the hypoplasticity theory (Kolymbas [25]). Mašín [26] provides a wide overview of the capabilities of the hypoplastic models, which include hypoplastic models for sands (Gudehus [27]; Von Wolffersdorff [28]) and their developments to account for small strain stiffness (Niemunis & Herle [29]) and reduction in the accumulation of strains in loading cycles (Wegener [30]; Wegener & Herle [31]).

The two families of constitutive approaches and the above-mentioned constitutive models and are not the only candidates to simulate cyclic soil behaviour. For example, Cudny & Truty [32] presented a constitutive model based on the approach of nested yield surfaces showing its implementation to be successful in replicating cyclic sand behaviour. In fact, the number of available soil constitutive models is greater and is still growing. On the other hand, although attempted for some models in certain aspects, detailed validation of the available advanced soil constitutive models regarding their accuracy for modelling seismic SSI is still rather rare. Some advanced soil constitutive models have been shown to replicate laboratory soil cyclic tests successfully, subsequently have been implemented in finite element codes and used to make predictions for large boundary value problems. For example, Martinelli et al. [33] and Miriano et al. [34] used SANISAND models to predict the seismic response of a pile and a retaining wall, respectively; Kowalczyk & Gajo [35] used an advanced elastoplastic model to analyse numerically the phenomena of natural frequency wandering of structures due to changes in pore pressures in saturated soil. Nevertheless, ideally before the constitutive models are used in predictive studies, another important step in the validation of soil constitutive models is their ability to replicate experimental data regarding complex boundary value problems, including large soil domains of varying characteristics and different types of SSI.

Some previous research has been dedicated to the validation of soil constitutive models based on comparisons of numerical predictions with benchmark experimental works in flexible soil containers. One of the first such studies by Gajo & Muir Wood [36] used a simple Mohr Coulomb model and an advanced soil constitutive Pastor-Zienkiewicz model (Pastor et al. [37]) to simulate shear stack tests of Dar [38]. The authors indicated a need to develop more reliable soil constitutive models, in particular a model able to account for dependency of strength and dilatancy on mean effective pressure. Similar conclusions were also found by others: a) firstly by Abate et al. [39] who tested seismic performance of a simple 'Cap-hardening Drucker Prager' model and the Severn-Trent model [16][17]; and b) later by Abate & Massimino [40] who compared a visco-linear elastic constitutive model again with the Severn-Trent model. These authors observed that the simple soil constitutive models proved to be unreliable and the Severn-Trent model was able to capture soil seismic response reasonably well. A large number of codes was verified in PRENOLIN (PREdiction of NOn-LINear soil behaviour) project which dealt with nonlinear site response (Régnier et al. [41]). The authors concluded that the numerous tested numerical tools were not consistent with each other and showed significant misfit with the measured observations of the site response. A different study by Bilotta et al. [42] summarized results of five different predicting teams in the numerical round robin competition for seismic simulations of a tunnel embedded in dry granular soil [10]. All teams were able to fairly well reproduce acceleration records in free field, both, in terms of the amplitudes and the frequency content. On the other hand, a consistent trend of underestimated settlement was shown by all five teams and the representation of bending moments and hoop forces in the embedded tunnel was captured only to a qualitative point. In addition to the mentioned studies, chosen advanced soil constitutive models were validated during the series of the LEAP projects. The summary of the numerical predictions for the LEAP-2017 project was provided by Manzari et al. [43] where the numerical codes were shown to perform generally well; however, some inconsistencies were still found in the site response of a sloping ground. In addition to [43], more detailed studies were shown by all the teams participating in the LEAP-2017 project. For instance, Ghofrani & Arduino [44] used one of the SANISAND models (Dafalias & Manzari model [18]) to model the site response and indicated that this soil constitutive model was capable to represent many aspects of saturated soil under seismic loading, but consideration of soil-structure interaction was missing in this validation.

To sum up, there is a substantial number of soil constitutive models aimed at simulating soil cyclic behaviour. Some of them have been implemented in the commercial finite element codes and used to analyse large boundary value problems studied previously in benchmark experimental works. Typically, the simulation of site response has been shown to be quite accurately captured by many numerical studies. On the other hand, comparisons focused on soil-structure interaction and structural response are rare, and if carried out, often show only qualitative agreement. Therefore, there is strong need for further validation of soil constitutive models, especially when focused on soil-structure interaction under seismic loading conditions.

The work presented in this paper shows validation of an advanced elastoplastic soil constitutive model, namely the Severn-Trent sand model in its most updated version (Gajo [45]), i.e. inclusive of a novel constitutive feature of a hyperelastic law inside the yield surface. The validation is carried out on examples of benchmark experimental work on soil-structure interaction of piles in dry soil (Durante [46]). Importantly, it is the first attempted detailed validation of the Severn-Trent sand model in the version proposed by Gajo [45], therefore this work is of high importance prior to adopting this soil constitutive model to reliable design and predicting tasks in seismic or offshore geotechnical engineering in the future. Generally successful comparisons of the numerical and experimental results are shown for two input motions and two different pile head conditions, including an experimental setup with a single degree of freedom (SDOF) structure on the top of one of the piles. Subsequently, the results are followed by short comments on two aspects of soil behaviour in shear stack experiments. Firstly, the potential origins of the high frequency components computed in the numerical studies and measured in the experimental work are briefly discussed. Secondly, the most important stress paths computed in the numerical study are detailed.

2. Methodology

This section presents details of the benchmark experimental work from literature (Durante [46]) adopted in this study (Section 2.1) to validate the soil constitutive model used in the finite element model (Section 2.2).

2.1 Benchmark experimental work on soil-structure interaction

2.1.1 Introduction to shear stack experiments

The experimental work in a flexible soil container used in this work as a benchmark experimental reference for the numerical study was carried out in the laboratory at the University of Bristol and was summarized by Chidichimo et al. [7], Simonelli et al. [8], Durante et al. [9] and Durante [46]. The history of the development of the flexible soil container, i.e. the shear stack container started with the works of Dar [38] and Crewe et al. [47]. The currently used shear stack consists of eight aluminium stacks put on top of each other with flexible rubber links in between (Figure 1) in order to allow soil to control the mechanical response in the soil-shear stack system subjected to shaking. The shear stack dimensions are: 1200mm length, 800mm height and 650mm width. The scaling laws between an experimental model and a real size prototype were given by Muir Wood et al. [5] and are not recalled here.

2.1.2 Soil Profile

The experimental work (Durante [46]) was carried out with Leighton Buzzard (LB) sand placed in the shear stack. Two different fractions of this sand were used, namely fraction E in the top 'softer' layer and a mixture of fractions B (85%) and E (15%) in the bottom 'stiffer' layer. The properties of LB sand and the soil profile in the shear stack are presented in Tables 1 and 2, respectively.

2.1.3 Pile and structure modelling

The experimental work (Durante [46]) comprised a five-pile group with different pile head conditions. These included free head piles, a short cap spanning the three closer piles (piles no. 1, 2 and 3), and a long cap spanning all five piles, all to simulate kinematic soil-structure interaction. The basic experimental setup is shown on Figure 2. In addition, some experimental runs included a SDOF oscillator placed on pile no.3 in order to simulate a structure and study inertial soil-structure interaction. The pile model was an aluminium tube of 750mm length, 22mm external diameter and 0.71mm wall thickness. The piles on their tops were equipped with a plastic cap with instrumentation (accelerometers, transducers) of a total mass approximated in this paper to be around 80gr. The structure was modelled as a 100mm long aluminium column of a rectangular section 3mm x 12mm and variable mass on the top of the column.

2.1.4 Monitoring instruments

The monitoring instrumentation included accelerometers, displacement transducers, strain gauges and an Indikon instrument to measure settlement. The placement of a part of the instrumentation from the experimental setup used in the result presentation of this paper is shown on Figure 3. The details of all data measurement channels are available in Durante [46].

All the measuring channels in the experiment were a subject to filtering procedure (lowpass Butterworth filter 80Hz, 5th order) in order to remove very high frequency experimental noise (Durante [46]).

2.1.5 Input motions

Two out of seven input acceleration time histories of moderate amplitudes analysed by the author in the past (Kowalczyk [50]) have been chosen in this study (note that the general conclusions on the reliability of the constitutive model are not dependent on this choice). The sinusoidal input motions and the pile head conditions analysed in this paper are shown in Table 3. The results expressed in terms of accelerations and displacements in this paper are shown for the steady state part of the response under harmonic excitation. Note that the experimentally and numerically applied input motions were introduced as sinusoidal cycles of steadily growing amplitude, thus the dynamic effects due to transient response are anyway reduced. Both cases shown in Table 3 comprise free pile head (FPH) conditions. The second analysed input motion is for the case of the pile no. 3 with a single degree of freedom (SDOF) oscillator on the pile top. The numerical analyses in this paper have focused solely on S-wave propagation, therefore accelerations throughout this paper should be explicitly understood as horizontal accelerations.

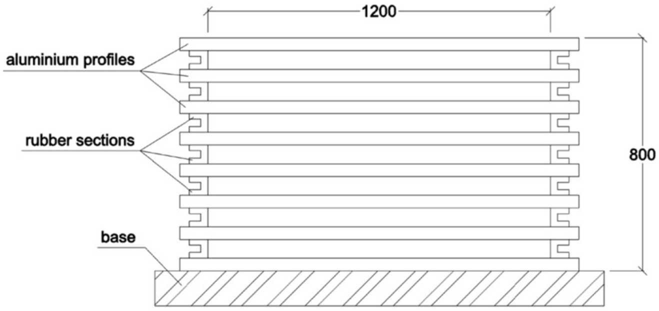

Figure 1. Sketch of longitudinal view of flexible soil container used in experimental work (dimensions in mm).

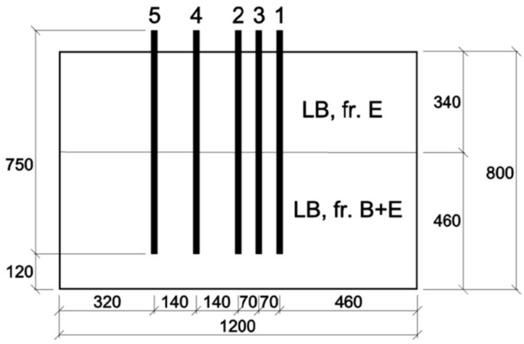

Figure 2. Geometry of basic experimental setup and pile numbering of pile group in shear stack as per Durante [46] (dimensions in mm).

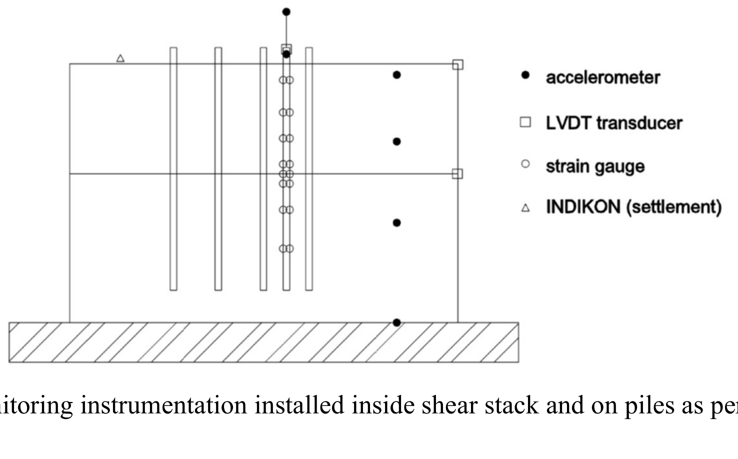

Figure 3. Part of monitoring instrumentation installed inside shear stack and on piles as per Durante [46].

Table 1. Properties of Leighton Buzzard (LB) sand used in the experiment by Durante [46].

Sand type	γ_s [kg/m3]	e_{min}	e_{max}	D_{10}	D_{50}	Reference
LB, fr. E	2647	0.613	1.014	0.095	0.14	Tan [48]
LB, fr. B+E	2647	0.289	0.614			Moccia [49]

Table 2. Properties of Leighton Buzzard (LB) sand within two soil layers modelled in the experiment by Durante [46].

Layer	height [m]	γ_s [kg/m3]	e	D_r [%]
LB, fr. E	0.46-0.8	1332	0.91	26
LB, fr. B+E	0-0.46	1800	0.48	41

Table 3. Chosen input motions and pile head conditions.

Case	Type of input motion	Maximum horizontal acceleration	Pile head conditions
I	Sine 25Hz	0.077g	FHP
II	Sine 10Hz	0.155g	FHP+SDOF

2.2 Finite element analysis

This section presents different aspects of the finite element model carried out in Abaqus (Dassault Systèmes [51]).

2.2.1 Soil constitutive model

The soil constitutive model used in this work belongs to the family of elastoplastic soil models. Its current formulation (Gajo [45]) and implementation (Gajo [52]) is a development of the Severn-Trent model by Gajo & Muir Wood [16][17]. The original formulation of the Severn-Trent model [16][17] was based on the bounding surface approach and showed a constitutive model capable for accounting for the well-known geotechnical concepts such as critical state, Mohr-Coulomb failure and current density and pressure measure in a form of the state parameter Ψ (Been & Jeffries [53]).

The updated version of the Severn-Trent model used in this work [45], instead of adopting the bounding surface approach, was formulated in an equivalent formulation of kinematic hardening elastoplasticity. Herein, the flow rule of the original model was updated to improve the predictions of volumetric compression observed typically under load reversals in cyclic loading. The plastic stiffness was defined as depending on the distance from the strength surface and on the Lode's angle in the deviatoric plane, thus two plastic stiffness parameters are needed (B_{min} and B_{max}). In addition, a 'smoothening' model parameter α was introduced to ensure smooth stiffness change between the elastic and the plastic stiffnesses. The most prominent feature of the updated formulation is a hyperelastic law within the yield surface instead of previously used simplified hypoelastic formulation. In general, hypoelasticity, although often used in constitutive modelling by many research groups, is not thermodynamically consistent, i.e. it can generate energy in the analysed system, thus may yield unreliable predictions. Instead of using the hypoelastic law, Gajo [45] derived the nonlinear elastic law from free energy density function φ:

$$\varphi(\boldsymbol{\varepsilon^e}, \boldsymbol{\varepsilon^p}) = \gamma d\big(-tr(\boldsymbol{B}\boldsymbol{\varepsilon}^e)\big)^{\eta} + \zeta d(tr(\boldsymbol{B}\boldsymbol{\varepsilon}^e)^2)^{\lambda} \qquad (1)$$

where: $\boldsymbol{\varepsilon^e}$ is elastic strain, $\boldsymbol{\varepsilon^p}$ is plastic strain, $\boldsymbol{B}$ is a fabric tensor (symmetric, second-order, positive-definite and dependent on plastic strain $\boldsymbol{\varepsilon^p}$) and d, γ, η, λ and ζ are constitutive parameters. In the original formulation tensor $\boldsymbol{B}$ describes developing fabric anisotropy due to plastic strains. In the model implementation used herein [52], tensor $\boldsymbol{B}=\boldsymbol{I}$, i.e. it is kept constant thus the initial anisotropy and the changes in anisotropy due to plastic strains are not accounted for; however, the implemented elastic law remains innovative, as thermodynamically consistent. More details regarding the formulation of the Severn-Trent model can be found in the referenced works.

To sum up, the Severn-Trent model in its current version is one of the most innovative constitutive approaches which has not been validated on large boundary value problems yet. Therefore, the presented work addresses this gap by detailed investigation of its performance regarding replicating seismic SSI.

2.2.2 Calibration of the constitutive model

No laboratory work on the small strain shear stiffness of LB sand (fraction E & fraction B+E) in low mean effective pressure is known to the author. Therefore, the calibration of the constitutive model has been based on the G/G_0 stiffness degradation with increasing strains derived for dry sands in low mean effective pressure in shear stack studies as per Dietz & Muir Wood [54]. Figure 4a shows the reference G/G_0 stiffness degradation curves from Dietz & Muir Wood [54] with limits as given by Seed & Idris [55]. These limits were also supported by similar G/G_0 trends obtained by Kokusho [56] who derived these for low mean effective stresses of approximately 20kPa. Therefore, such choice for the calibration of the constitutive models can be deemed suitable.

Figure 4b shows the G/G_0 curves predicted by the constitutive model when evaluated at low mean effective pressure in simple shear. Generally, the calibration of the constitutive model fits well within the limits specified by Seed & Idris [55] and remains close to the G/G_0 curves established by Dietz & Muir Wood [54] and Kokusho [56], thus reliable simulations can be expected.

The model calibration input parameters are listed in Table 4. The performance of the constitutive model with this set of input parameters and adjusted void ratio to model different sand is shown on Figure 5 when simulating experimental laboratory tests on Toyoura sand [57]. The constitutive model is shown to capture the compressive behaviour and the slight increase in stiffness and strength observed with loading cycles when simulating the cyclic simple shear test [57].

Note that the two soil layers in the shear stack experiments (LB, fr. E and LB, fr. B+E) have been modelled using the same set of model input parameters. The only difference between the two layers lied in: a) the initial void ratio which has been chosen to be 0.91 (top layer) and 0.85 (bottom layer) in order to achieve relative densities of 26% and 41% as per the experiments (Table 2), b) weight of soil (also as per Table 2). Although such modelling approach is a simplification it was shown in the past to be successful in case of simulating different sands with a single set of model parameters and equivalent void ratio (e.g. for Hostun and Toyoura sands by Gajo [45]).

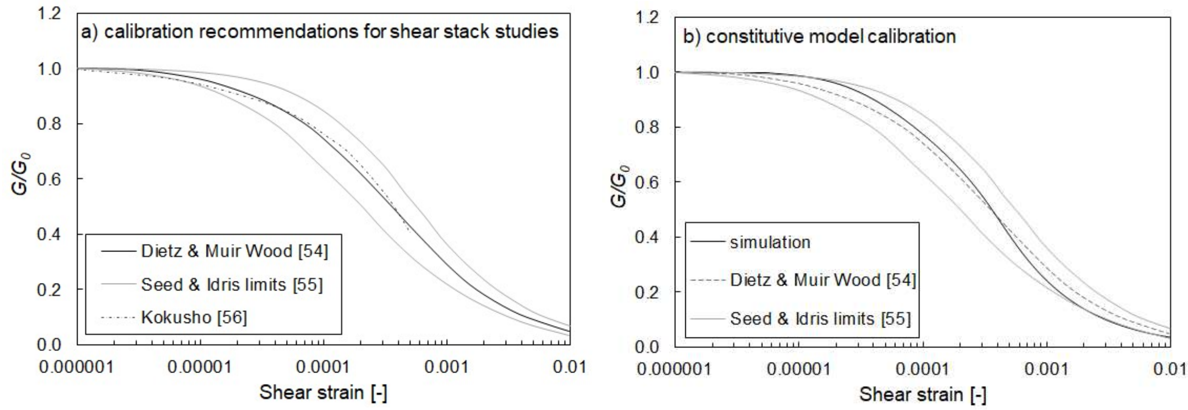

Figure 4. Calibration of stiffness degradation curves G/G_0: a) recommendations for shear stack studies, b) constitutive model calibration.

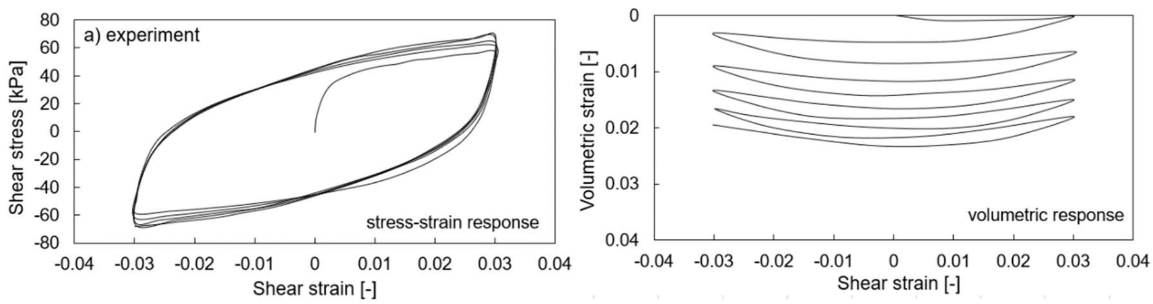

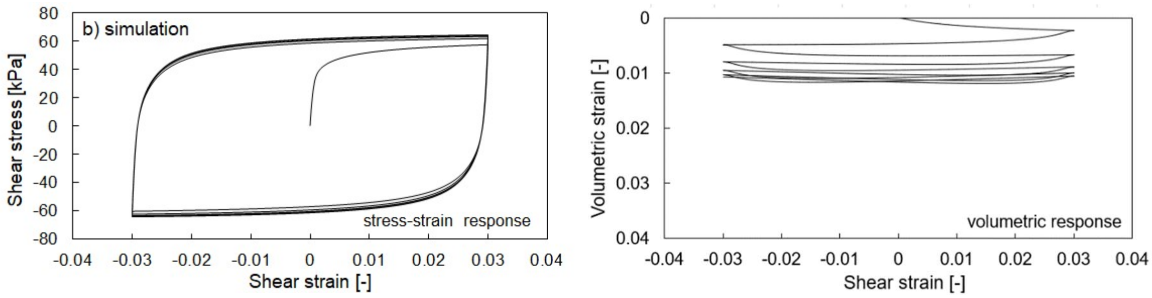

Figure 5. Comparison of cyclic simple shear test on Toyoura sand at p'=100kPa: a) experimental measurements by Shahnazari & Towhata [57] with e_{init}=0.756, b) simulations with e_{init}=0.9.

Table 4. Input parameters for the constitutive model

Parameter	Description	Value
v_{Δ}	Intercept for critical-state line in v-ln p plane at p=1Pa	2.194
Δ	Slope of critical-state line in v-ln p plane	0.0267
φ_{cv}	Critical-state angle of friction	33°
m	Parameter controlling deviatoric section of yield surface	0.8
k	Link between changes in state parameter and current size of yield surface	3.5
A	Multiplier in the flow rule	0.75
k_d	State parameter contribution in flow rule	1.3
B_{min}	Parameter controlling hyperbolic stiffness relationship	0.0005
B_{max}	Parameter controlling hyperbolic stiffness relationship	0.002
α	Exponent controlling hyperbolic stiffness relationship	1.6
R_R	Size of the yield surface with respect to the strength surface	0.02/0.01*
E_R	Fraction of G_0 used in the computations	1.0

* slightly larger yield surface has been assumed in the top soil layer to avoid numerical problems at shallow depths in the region of very low mean effective pressures

2.2.3 Soil geometry and discretization

The optimal mesh used in the 3D numerical studies together with the reference elements chosen for the result presentation is shown on Figure 6. Due to the symmetry in the model, only half of the shear stack has been modelled in order to reduce the computational costs.

Periodic boundaries have been defined on the lateral sides of the mesh through tie connectors between the side nodes. Two approaches are typical when tying the side nodes, one restricting all degrees of freedom [e.g. Gajo & Muir Wood [36]), and second, probably more common, assuming restricting only horizontal movement thus allowing vertical movement on both sides to differ (e.g. Abate et al. [39]). In fact, the author in his previous work [50] constrained all degrees of freedom since the experimental data (Durante [46]) identified unaffected response in free field and no presence of horizontally propagating surface waves. Instead in this work, the second approach was chosen as possibly more widely accepted among geotechnical research community. In any case, this choice does not significantly affect the results of the validation of the constitutive model, as one can see by comparisons of the results reported in this work with the results presented in (Kowalczyk [50]).

Seismic input motion has been applied as an acceleration time history of a single sine frequency (i.e. 'perfectly sinusoidal') at the bottom of the mesh. No dissipative boundaries have been defined at the bottom of the mesh as wave reflection is expected to be experienced in the shear stack placed on a rigid shaking table. The effect of aluminium stacks has been omitted as typically considered of negligible influence (Gajo & Muir Wood [36]; Dietz & Miur Wood [54]).

The element type for soil is a quadratic ‘brick’ element from the library of Abaqus elements (Dassault Systèmes [51]). The element size has been calculated from the elastic wave propagation for the slowest wave (i.e. G_0 of around 3MPa in superficial soil) and highest frequency (80Hz to account for most important higher frequencies). This resulted in a maximum distance between two nodes to be 0.06m, which has been subsequently reduced to 0.025m (quadratic element size 0.05m) in order to account for plasticity developing in soil at shallower depths and therefore slower waves propagating as advised by Watanabe et al. [58]. Moreover, the ratio of the element size to the pile diameter remains within the limits of similar finite element numerical studies (e.g. Martinelli et al. [33]).

The numerical results for the computed accelerations have been filtered, i.e. a lowpass Butterworth filter 80Hz (5th order) has been used for the sake of consistency with the experimental data.

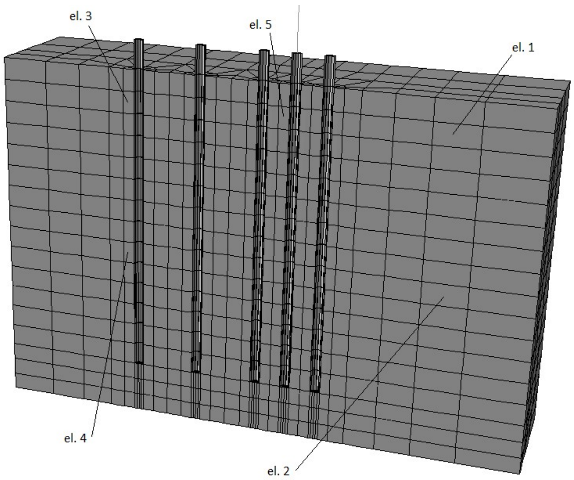

Figure 6. Final optimal 3D mesh discretization for the case II (Table 3) with chosen reference elements for presentation of results.

2.2.4 Pile geometry and discretization

A shell element type has been chosen to model the tubular piles of 22mm diameter and 0.71mm wall thickness. The piles have been modelled with an elastic material representative of aluminium, i.e. with stiffness E=70GPa and Poisson’s ratio ν=0.3.

The soil-pile interface has been defined as frictional with an allowance for a gap opening. The coefficient of friction has been assumed to be 0.5 which is a typical value measured between granular soil and steel piles (e.g. Uesugi & Kishida [59]).

In addition, a mass of 80gr has been modelled at the top of the piles in order to account approximately for the mass of the accelerometer and the plastic cap.

2.2.5 Oscillator geometry and discretization

The single degree of freedom oscillator has been modelled as a 100mm long column of aluminium material and with a mass of 190gr at the top (to simulate the oscillator mass) and a mass of 176gr at the bottom (to simulate the foundation mass). The fixed-base natural frequency of such oscillator is 26.5Hz as experimentally assessed before (Durante [46]). Note that both masses were input as halves of the indicated values due to the fact of modelling only a half of the shear stack. The oscillator has been discretized with a beam element type of a rectangular aluminium section 3x6mm (half of the actual size 3x12mm) to be representative of the experimental setup (Durante [46]).

3. Results

The numerical results are presented in two sections depending on the applied input motion (see Table 3) and the absence (case I) or presence (case II) of a simplified structure in the form of a SDOF oscillator. The results for the pile are referred to pile no.3 within the five-pile group (Figure 2). Note that only the steady state response to harmonic sinusoidal excitation is shown herein, thus part of the motion up to 0.2sec relevant to transient response is generally omitted (shown only for settlement calculations).

3.1 Free head piles without oscillator (case I)

A comparison of the numerical and experimental results for the 25Hz input motion is presented in this section. The response in free field in terms of horizontal accelerations (Figure 7) and lateral relative displacements (Figure 8) is generally well simulated by the constitutive model. The computed accelerations capture the measured accelerations in terms of the amplitude and the phase shift between the input at the base and the motion at the top. Moreover, the distortion from the perfect sinusoidal input motion applied at the base can be clearly observed at the top in the experiment and the simulation, indicating the presence of high frequency components. The lateral relative displacements of soil are fairly accurately represented at two depths of the shear stack. On the other hand, the computed settlements (Figure 9) are overestimated in the simulations. Nevertheless, although the constitutive model overestimates compression, this remains relatively small (<1mm) and on overall have negligible effect on other computational trends.

Regarding the pile response, the computed accelerations (Figure 10) match very well the experimental measurements in terms of the maximum amplitude. The constitutive model also indicates the presence of high frequencies observed on the pile tops in the experiments. This effect has been reasonably well captured in the simulations. More comments on high frequencies will be subject to further discussion in Section 3.3 of the results.

Looking at the pile head lateral relative displacements (Figure 11) some minor inconsistency can be observed between the numerical and experimental studies. The pile lateral displacements seem to be slightly underestimated in the numerical simulations, nevertheless the order of magnitude is maintained. The slight misfit here could be due to the approximate estimation of the mass of 80gr at the top of the pile.

Finally, the pile maximum axial strains (representative of the pile maximum bending moments) are compared on Figure 12. Although, some discrepancies can be observed, in general, the computed values are within the order of magnitude of the experimental measurements and at similar depths.

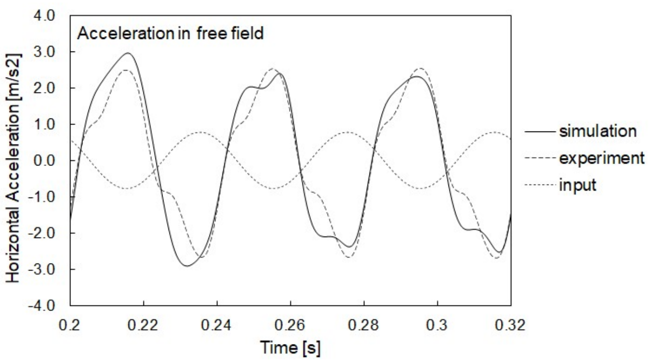

Figure 7. Comparison of measured and computed horizontal accelerations in free field at soil surface for case I.

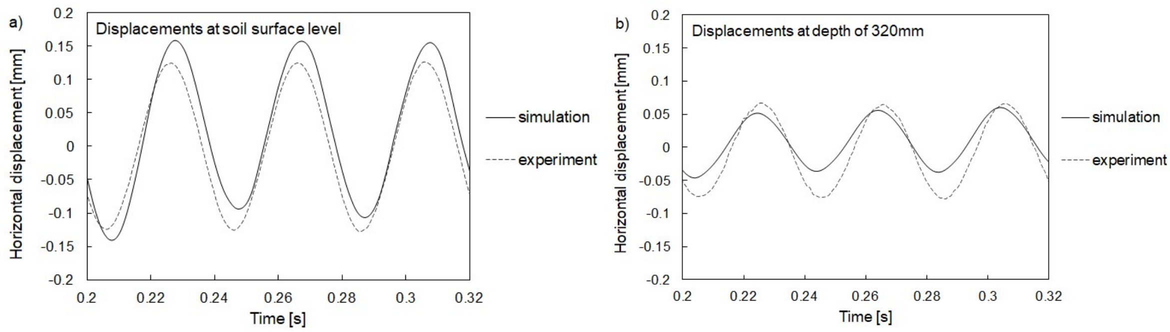

Figure 8. Comparison of measured and computed lateral relative displacements in free field: a) at soil surface level and b) at mid-height for case I.

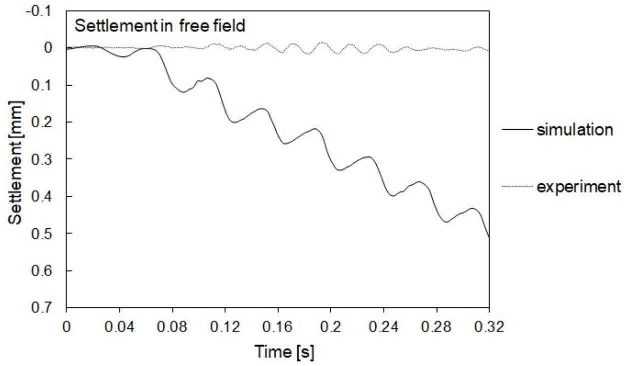

Figure 9. Comparison of measured and computed settlements at soil surface level for case I.

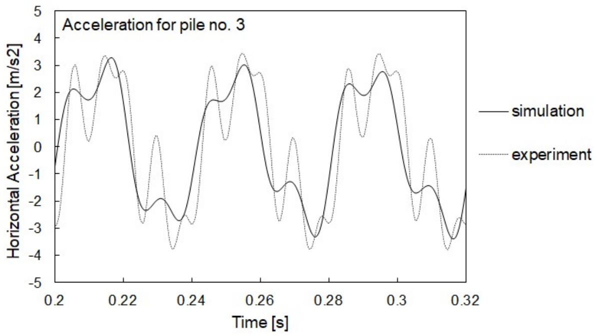

Figure 10. Comparison of measured and computed horizontal accelerations at top of pile no.3 for case I.

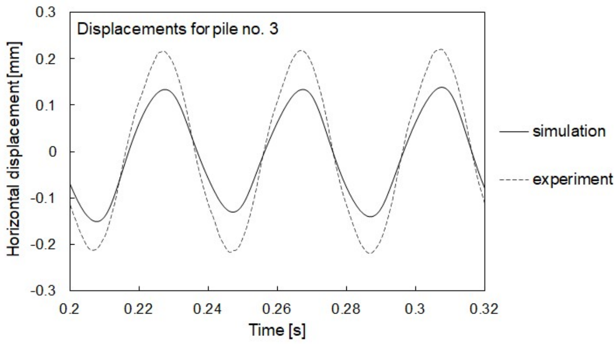

Figure 11. Comparison of measured and computed lateral relative displacements at top of pile no. 3 for case I.

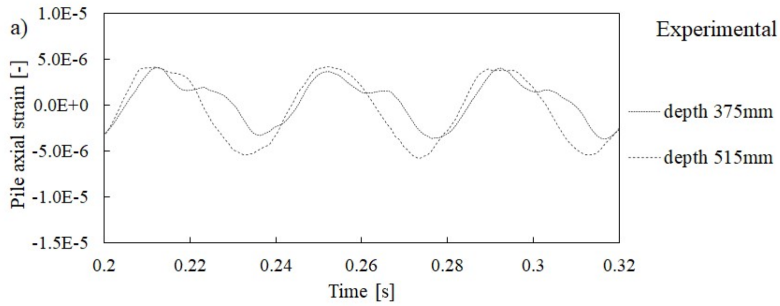

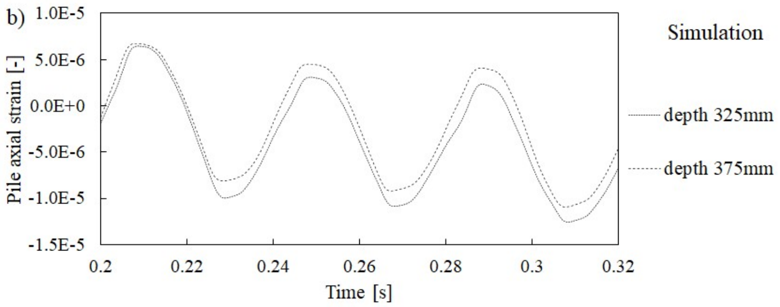

Figure 12. Comparison of maximum measured and computed pile axial strains of pile no. 3 in: a) experiment, b) simulation for case I.

3.2 Free head piles with oscillator (case II)

This section shows the results for the input motion of 10Hz sine dwell (Table 3) with free pile head conditions and a SDOF oscillator placed at the top of pile no. 3.

Firstly, the response in free field is compared (Figures 13-15). Generally, the accelerations in free field (Figure 13) are matched very well in terms of the computed amplitudes and fairly well in terms of the phase shift. The presence of high frequencies generated in soil is apparently overestimated in the simulations. The computations replicate in an accurate manner the lateral relative displacements at mid-depth and with a slight misfit at soil surface level (Figure 14). The computed settlements (Figure 15) are overestimated again by the constitutive model; however, the total magnitude remains relatively small, similarly to the case shown in Section 3.1.

The horizontal accelerations of pile no. 3 are shown on Figure 16 and are in fairly good agreement between the computations and the experiments, with stronger presence of high frequencies in the numerical studies. The pile lateral relative displacements and the pile maximum axial strains are shown on Figures 17 and 18, respectively. The lateral relative displacements of the pile match very well those measured in the experiment. In addition, to the correctly predicted amplitude, the computed and measured lateral displacements show slight distortion from perfect sinusoidal motion, thus indicating again the presence of high frequencies. The maximum pile axial strains are measured and computed around the top of the pile, with the numerical model slightly underestimating the amplitude of the measured axial strains. The presence of the apparent high frequency motion is stronger again in the numerically computed pile axial strains than those observed experimentally.

Finally, the computed accelerations at the top of the SDOF oscillator (Figure 19) show precise match with the maximum measured acceleration amplitudes. Generally, high frequencies are present in the motion of the oscillator in the numerical and experimental studies; although, their amount has not been captured very accurately in the simulations.

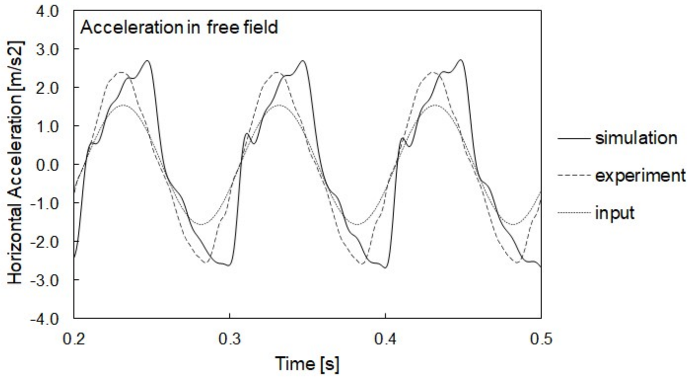

Figure 13. Comparison of measured and computed horizontal accelerations in free field at soil surface for case II.

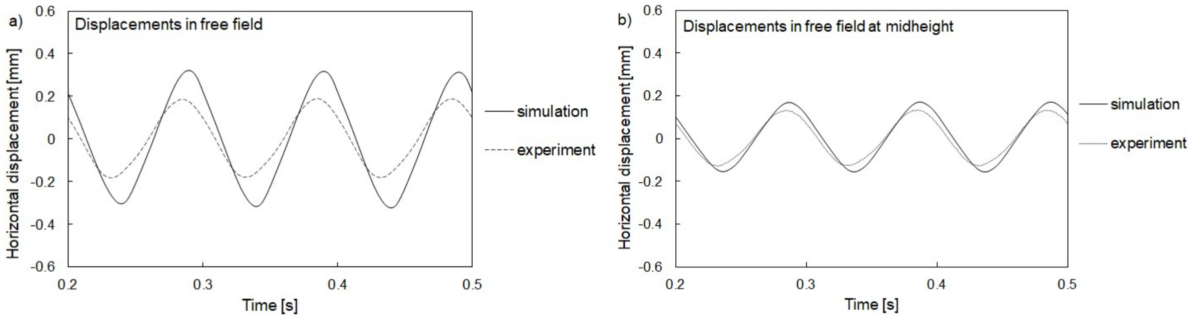

Figure 14. Comparison of measured and computed lateral displacements in free field: a) at soil surface level and b) at mid-height for case II.

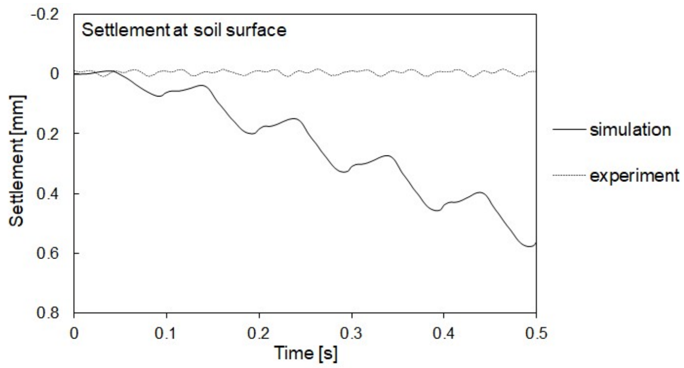

Figure 15. Comparison of measured and computed settlements at soil surface level for case II.

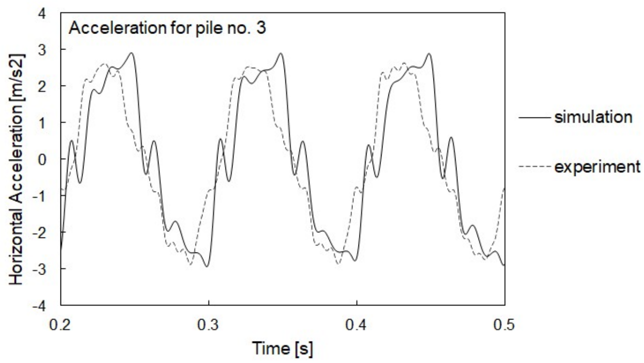

Figure 16. Comparison of measured and computed horizontal accelerations at top of pile no.3 for case II.

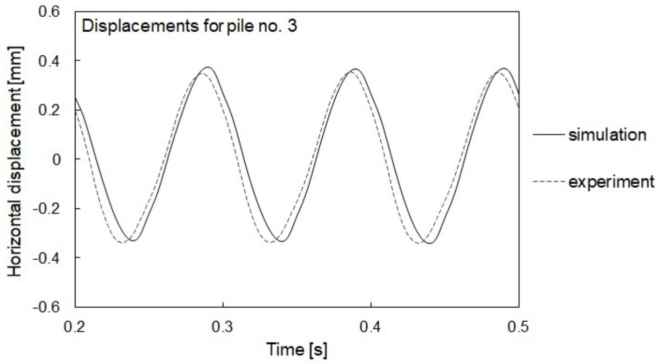

Figure 17. Comparison of measured and computed lateral relative displacements at top of pile no. 3 for case II.

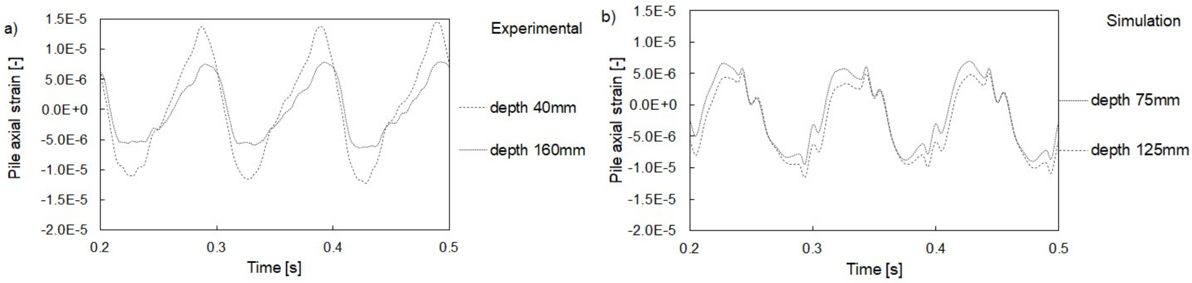

Figure 18. Comparison of maximum measured and computed pile axial strains of pile no. 3 in: a) experiment, b) simulation for case II.

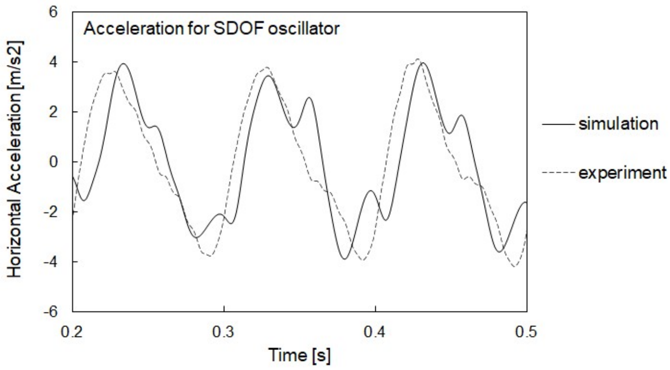

Figure 19. Comparison of measured and computed horizontal accelerations at top of oscillator for case II.

3.3 Comments on the presence of high frequencies

In general, the horizontal acceleration records (primarily) and the lateral relative displacements (to lower extent) presented in this paper show distortion from perfectly sinusoidal motion when inspecting the response in free field in soil and, especially, on piles. This is observed even though the applied input motions were perfectly sinusoidal when induced at soil base (in fact, even the experimentally applied input motion contained only fractional amount of higher harmonics, thus practically can be considered as perfectly sinusoidal).

The phenomenon of the presence of high frequencies in the steady state response was shown as potentially related to the general propagation of soil elastic unloading waves (Kowalczyk [50]), corrected subsequently to the propagation of soil elastic waves released upon unloading and ‘trapped’ in a soil column modelled by a simple nonlinear hysteretic constitutive model (Kowalczyk & Gajo [60]). The latter work suggests potential gaps in the theory of wave propagation in the materials of hysteretic stress-strain behaviour showing how soil elastic waves can be released upon unloading in soil in the steady state response leading to high frequency motion being observed. In the work presented herein, high frequencies can be representative of sinusoidal wave distortion and actual high frequency waves apparently generated in soil and affecting the structural response. In general, such behaviour, when a pile or a structure appears to amplify the soil-generated high frequency motion, may even lead towards a resonance between the structural natural frequency with the soil elastic waves as shown in a different work of the author [61].

Note that in the case of the presented work, it is difficult to identify unanimously the actual origin of the high frequencies observed in the experimental work from literature [46]. Although there are some initial proofs [60-61] pointing out on the potential presence of soil elastic waves released upon unloading, one should not forget that additional waves in the analysed system could possibly be induced in other manners, for example as a result of wave reflections on the interface of the bi-layered soil profile, wave scattering from the piles, or impact of the boundaries, i.e. interaction of soil with the soil container. Therefore, further research is needed, possibly with re-reviewing previous experimental works (e.g. [38]), to clearly identify the origin of the high frequency motion in similar experimental works.

3.4 Stress-strain behaviour in simulations of soil

This section presents the most representative stress-strain behaviours in the shear stack simulations in the chosen five reference elements from the 3D mesh (Figure 6) in their middle Gauss points for the 10Hz sine input motion with a SDOF structure on the top of the pile no. 3 (Section 3.2). The reference elements can be divided in three zones, representing free field (elements no. 1 and 2), vicinity of a pile under kinematic loading (elements no. 3 and 4) and vicinity of a pile with a SDOF structure (element no. 5).

Figure 20 depicts curves of shear stress normalized by vertical stress against shear strain computed by the constitutive model for the five chosen elements. Elements no. 1, 2 and partly element no. 4 (Figure 21a, b and d, respectively) show hysteretic fairly smooth behaviour almost as in simple shear tests, i.e. as expected in free field or close to the pile but at depth where piles under kinematic loading are fully driven by soil behaviour. On the other hand, elements no. 3 (Figure 21c) and especially no. 5 (Figure 21e) show more erratic stress strain curves. In these regions, the response is no longer dominated by the simple shear type of behaviour since the impact from the relatively stiffer pile with a smaller mass (element no. 3) or larger mass (element no. 5) becomes dominant. In addition, note that it appears that the soil constitutive model predicts response with some accumulation of shear strains. Nevertheless, this ‘ratcheting’ behaviour apparently does not affect significantly the global response when comparing with the experiments. In fact, some accumulation of plastic shear strain would also be expected in the experiments.

Figure 21 shows lateral loading in terms of the stress ratio σ_h/σ_v versus lateral strain on soil elements 1 and 5, respectively. The σ_h in the stress ratio is to be understood as horizontal stress in the direction of the applied shaking (similarly lateral strain is horizontal strain in the direction of the applied shaking). Based on the computed stress-strain behaviour, it can be observed that the lateral type of loading is of less importance in free field (Figure 21a) but it can be of increased importance for the pile with an oscillator on its top (Figure 21b). The large variations in the stress ratio σ_h/σ_v would be expected to be potentially important when investigating the fabric effects on changes in the small strain stiffness, i.e. changes in stiffness anisotropy [62]. Note that the computed variations in the stress ratio σ_h/σ_v from 0.3 to up to 1.4 shown here, come from moderate-level input motions (i.e. maximum of 0.155g) and would be expected to decrease below 0.3 and increase beyond 1.4 for higher intensity seismic events.

Note that the computed and shown here stress strain curves for the analysed input motions apparently do not show any ‘overshooting’ in the predictions of soil stiffness and strength on reloading, i.e. common limitation of many soil constitutive models, including the Severn-Trent model, as shown by the author in his previous work [50].

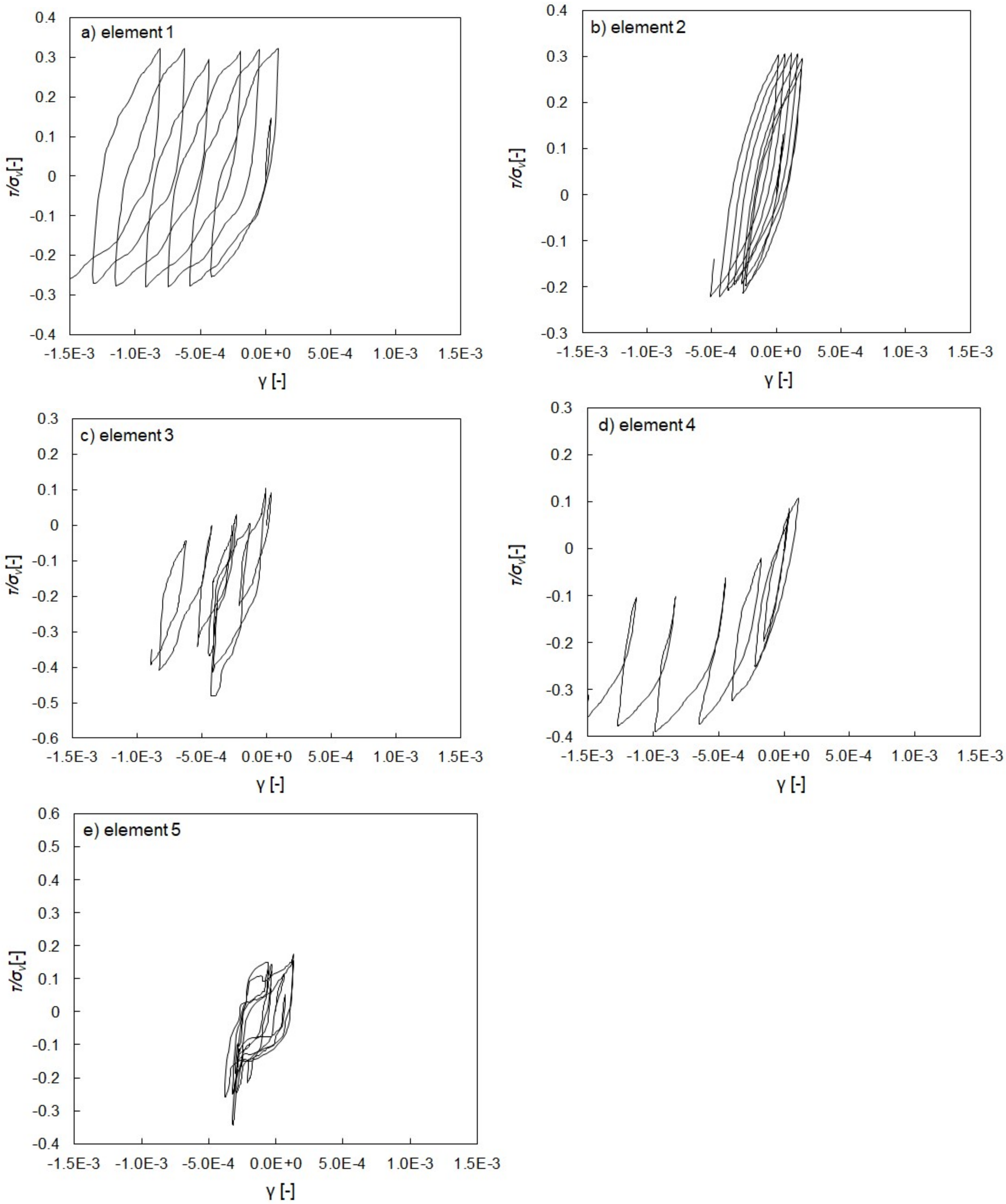

Figure 20. Shear stress strain behaviour in: a) element no. 1 in free field at around 90mm depth, b) element no. 2 in free field at around 430mm depth, c) element no. 3 in vicinity of kinematic pile at around 90mm depth, d) element no. 4 in vicinity of kinematic pile at around 430mm depth, e) element no. 5 in vicinity of kinematic pile with SDOF structure at around 90mm depth.

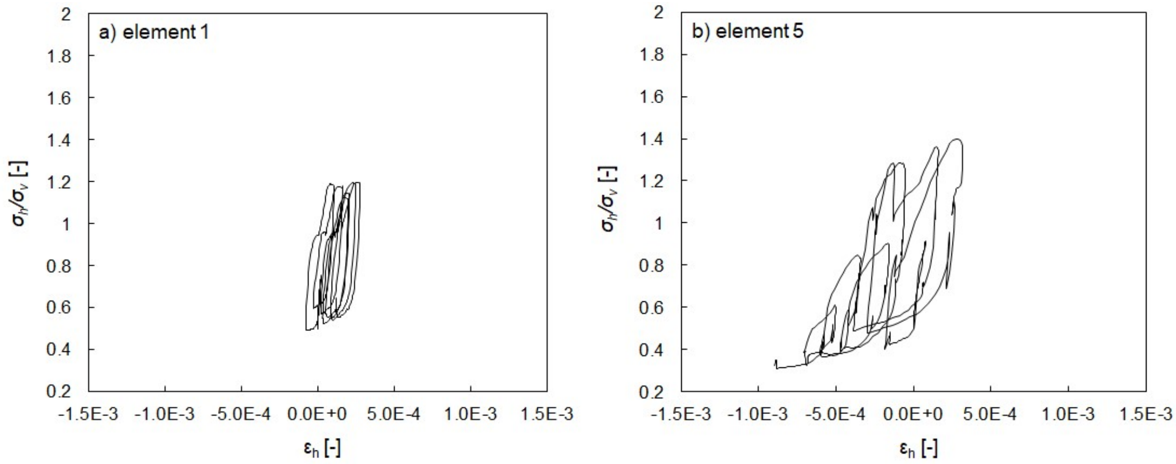

Figure 21. Stress ratio (σ_h/σ_v) versus horizontal axial strain curves for: a) element no. 1 at around 90mm depth, b) element no. 5 in vicinity of kinematic pile with SDOF structure at around 90mm depth.

4. Summary

This paper has presented validation of an advanced sand constitutive model (Gajo [45]) on benchmark experimental work on soil-structure interaction (Durante [46]). It has been shown that the investigated sand constitutive model is capable of simulating seismic soil behaviour and seismic soil-structure interaction at least qualitatively, and in most cases with high accuracy. The comparisons with experimental data included free field response, kinematic and inertial soil-structure interaction under two input motions and two different pile head conditions. Free field response in terms of the computed accelerations and displacements has been generally very well captured, whereas some discrepancies have been encountered when predicting settlements and sporadically, when analysing structural response. The origin of the observed high frequencies in the computations and experiments has been briefly discussed. Finally, the most important stress paths experienced in soil have been highlighted based on the conducted computations.

Funding:

The research presented herein has been initiated under the XP-Resilience project. This project received funding from the European Union’s Horizon 2020 research and innovation programme under the Marie Skłodowska-Curie grant agreement No 721816.

Acknowledgments:

The author would like to thank Dr Maria Giovanna Durante (University of Texas) and Professor Luigi Di Sarno (University of Liverpool) for providing examples of raw experimental data of the benchmark shear stack experiments on soil-structure interaction. Special further thanks to Dr Maria Giovanna Durante for brief but fruitful email exchange regarding experimental details.

The author thanks Professor Alessandro Gajo (University of Trento) for the provision of the numerical tools, advice and support during the PhD research of the author where the work presented in this manuscript was commenced, and for the revision and valuable comments to the draft of this manuscript.

The author would also like to acknowledge an anonymous reviewer for little adjustments and suggestions to the manuscript.

References

1. Pitilakis, D., Dietz, M., Muir Wood, D., Clouteau, D., Modaressi, A. (2008). Numerical simulation of dynamic soil-structure interaction in shaking table testing. *Soil Dyn Earthq Eng* 28, 453-467. https://doi.org/10.1016/j.soildyn.2007.07.011

2. Loli, M., Apostolou, M., Gazetas, G., Gerolymos, N., Anastasopoulos, I. (2010). Soil failure can be used for seismic protection of structures. *Bull Earthquake Eng* 8: 309-326. https://doi.org/10.1007/s10518-009-9145-2
3. Hall, J. F., Beck, J. L (1986). Structural damage in Mexico City. *Geophys Res Lett*, 13(6), 589-592. https://doi.org/10.1029/GL013i006p00589
4. Mylonakis, G., Gazetas, G. (2000). Seismic soil-structure interaction: beneficial or detrimental? *J Earthq Eng*, 4(3), 277-301. https://doi.org/10.1080/13632460009350372
5. Muir Wood, D., Crewe, A., Taylor, C. (2002). Shaking table testing of geotechnical models. *Int J Phys Model* 1: 01-13. https://doi.org/10.1680/ijpmg.2002.020101
6. Massimino, M. R., Maugeri, M. (2013). Physical modelling of shaking table tests on dynamic soil-foundation interaction and numerical and analytical simulation. *Soil Dyn Earthq Eng* 49: 1-18. https://doi.org/10.1016/j.soildyn.2013.01.023
7. Chidichimo, A., Cairo, R., Dente, G., Taylor, C. A., Mylonakis, G. (2014). 1-g experimental investigation of bi-layer soil response and kinematic pile bending. *Soil Dyn Earth Eng* 67, 219-232. https://doi.org/10.1016/j.soildyn.2014.07.008
8. Simonelli, A. L., Di Sarno, L., Durante, M. G., Sica, S., Bhattacharya, S., Dietz, M., Dihoru, L., Taylor, C. A., Cairo, R., Chichidimo, A., Dente, G., Modaressi, A., Todo Bom, L. A., Kaynia, A. M., Anoyatis, G., Mylonakis, G. (2014). Experimental assessment of seismic pile-soil interaction. Chapter 26. Seismic evaluation and rehabilitation of structures.
9. Durante, M. G., Di Sarno, L., Mylonakis, G., Taylor, C. A., Simonelli, A. L. (2016). Soil-pile-structure interaction: experimental outcomes from shaking table tests. *Earthq Eng Struct Dyn*, 45(7), 1041-1061. https://doi.org/10.1002/eqe.2694
10. Lanzano, G., Bilotta, E., Russo, G., Silvestri, F., Madabushi, S. P. G. (2012). Centrifuge modelling of seismic loading on tunnels in sand. *Geotech Test J* 35(6), 854-869. https://doi.org/10.1520/GTJ104348
11. Conti, R., Madabhushi, G. S. P., Viggiani, G. M. B. (2012). On the behavior of flexible retaining walls under seismic actions. *Géotechnique* 62(12), 1081-1094. https://doi.org/10.1680/geot.11.P.029
12. Kutter, B. L., Carey, T. J., Hashimoto, T., Zeghal, M., Abdoun, T., Kokkali, P., Madabhushi, G., Haigh, S. K., Burali d'Arezzo, F., Madabhushi, S., Hung, W.-Y., Lee, C.-J., Cheng, H.-C., Iai, S., Tobita, T., Ashino, T., Ren, J., Zhou, Y.-G., Chen, Y.-M., Sun, Z.-B., Manzari, M. T. (2018). LEAP-GWU-2015 experiment specifications, results and comparisons. *Soil Dyn Earthq Eng* 113, 616-628. https://doi.org/10.1016/j.soildyn.2017.05.018
13. Kutter, B. L., Carey, T. J., Stone, N., Li Zheng, B., Gavras, A., Manzari, M. T., Zeghal, M., Abdoun, T., Korre, E., Escoffier, S., Haigh, S. K., Madabushi, G. S. P., Madabushi, S. S. C., Hung, W.-Y., Liao, T.-W., Kim, D.-S., Kim, S.-N., Ha, J.-G., Kim, N. R., Okamura, M., Sjafruddin, A., N., Tobita, T., Ueda, K., Vargas, R., Zhou, Y.-G., Liu, K. (2019). LEAP-UCD-2017 Comparison of Centrifuge Test Results. *In: B. Kutter et al. (Eds.), Model tests and numerical simulations of liquefaction and lateral spreading: LEAP-UCD-2017*. New York: Springer.
14. Tokimatsu, K., Suzuki, H., Sato, M. (2005). Effects of inertial and kinematic interaction on seismic behaviour of pile with embedded foundation. *Soil Dyn Earthq Eng* 25(7-10), 753-762. https://doi.org/10.1016/j.soildyn.2004.11.018
15. Shirato, M., Nonomura, Y., Fukui, J., Nakatani, S. (2008). Large-scale shake table experiment and numerical simulation on the nonlinear behaviour of pile-groups subjected to large-scale earthquakes. *Soils Found* 48(3), 375-396. https://doi.org/10.3208/sandf.48.375
16. Gajo, A., Muir Wood, D. (1999a). Severn-Trent sand: a kinematic hardening constitutive model for sands: the q-p formulation. *Géotechnique* 49(5), 595-614. https://doi.org/10.1680/geot.1999.49.5.595
17. Gajo, A., Muir Wood, D. (1999b). A kinematic hardening constitutive model for sands: the multiaxial formulation. *Inter J Numer Anal* 23(9), 925-965. https://doi.org/10.1002/(SICI)1096-9853(19990810)23:9<925::AID-NAG19>3.0.CO;2-M
18. Dafalias, Y., F., Manzari, M. T. (2004). A simple plasticity sand model accounting for fabric change effects. *J Eng Mech* 130(6), 622-634. https://doi.org/10.1061/(ASCE)0733-9399(2004)130:6(622)
19. Dafalias, Y., F., Papadimitriou, A. G., Li, X. S. (2004). Sand plasticity model accounting for inherent fabric anisotropy. *J Eng Mech* 130(11): 1319-1333. https://doi.org/10.1061/(ASCE)0733-9399(2004)130:11(1319)

20. Taiebat, M., Dafalias, Y. F. (2008). SANISAND: Simple anisotropic sand plasticity model. *Inter J Numer Anal* 32, 915-948. https://doi.org/10.1002/nag.651
21. Dafalias, Y., F., Taiebat, M. (2016). SANISAND-Z: zero elastic range sand plasticity. *Geotechnique*, 66(12), 999-1013. https://doi.org/10.1680/jgeot.15.P.271
22. Manzari, M. T., Dafalias, Y. F. (1997). A critical state two-surface plasticity model for sands. *Géotechnique* 47(2), 255-272. https://doi.org/10.1680/geot.1997.47.2.255
23. Pisano, F., Jeremic, B. (2014). Simulating stiffness degradation and damping in soils via a simple visco-elastic-plastic model. *Soil Dyn and Earthq Eng* 63, 98-109. https://doi.org/10.1016/j.soildyn.2014.02.014
24. Boulanger, R., Ziotopoulou, K. (2015). PM4Sand Version 3: A sand plasticity model for earthquake engineering applications. Technical Report.
25. Kolymbas, D. (1991). Computer-aided design of constitutive laws. *Inter J Numer Anal* 15, 593-604. https://doi.org/10.1002/nag.1610150806
26. Mašín, D. (2018). *Modelling of soil behaviour with hypoplasticity. Another approach to soil constitutive modelling*. Springer.
27. Gudehus, G. (1996). A comprehensive constitutive equation for granular materials. *Soils Found* 36(1), 1-12. https://doi.org/10.3208/sandf.36.1
28. Von Wolffersdorff, P. A. (1996). A hypoplastic relation for granular materials with a predefined limit state surface. *Mech Cohesive Frict Mater* 1(3), 251-271. https://doi.org/10.1002/(SICI)1099-1484(199607)1:3<251::AID-CFM13>3.0.CO;2-3
29. Niemunis, A., Herle, I. (1997). Hypoplastic model for cohesionless soils with elastic strain range. *Mech Cohesive Frict Mater 2*, 279-299. https://doi.org/10.1002/(SICI)1099-1484(199710)2:4<279::AID-CFM29>3.0.CO;2-8
30. Wegener, D. (2013). Numerical investigation of permanent displacements due to dynamic loading. *PhD thesis*. Publications of the Institut fur Geotechnik at the TU Dresden, no. 17.
31. Wegener, D., Herle, I. (2014). Prediction of permanent soil deformations due to cyclic shearing with a hypoplastic constitutive model. *Geotechnik* 37(2), 113-122. https://doi.org/10.1002/gete.201300013
32. Cudny, M., Truty, A. (2020) Refinement of the Hardening Soil model within the small strain range. *Acta Geotech* 15: 2031–2051 https://doi.org/10.1007/s11440-020-00945-5
33. Martinelli, M., Burghignoli, A., Callisto, L. (2016) Dynamic response of a pile embedded into a layered soil. *Soil Dyn and Earthq Eng* 87:16-28. https://doi.org/10.1016/j.soildyn.2016.03.021
34. Miriano, C., Cattoni, E., Tamagnini, C. (2016) Advanced numerical modelling of seismic response of a propped r.c. diaphragm wall. *Acta Geotech* 11(1): 161-175. https://doi.org/10.1007/s11440-015-0378-8
35. Kowalczyk, P., Gajo, A. (2021) Influence of pore pressure on natural frequency wandering of structures under earthquake conditions. *Soil Dynamics & Earthquake Engineering* 142. https://doi.org/10.1016/j.soildyn.2020.106534
36. Gajo, A., Muir Wood, D. (1997). Numerical analyses of behaviour of shear stacks under dynamic loading. Report on work performed under the EC project European Consortium of Earthquake Shaking Tables (ECOEST): Seismic bearing capacity of shallow foundations.
37. Pastor, M., Zienkiewicz, O.C., Chan, A.H.C. (1990). Generalized plasticity and the modelling of soil behaviour. *Inter J Numer Anal* 14, 151-190. https://doi.org/10.1002/nag.1610140302
38. Dar, A. R. (1993). Development of a flexible shear-stack for shaking table testing of geotechnical problems. *PhD Thesis*. University of Bristol.
39. Abate, G., Massimino, M., R., Maugeri, M., Muir Wood, D. (2010). Numerical modelling of a shaking table test for soil-foundation-superstructure interaction by means of a soil constitutive model implemented in a FEM Code. *Geotech and Geol Eng* 28(1), 37-59. https://doi.org/10.1007/s10706-009-9275-y
40. Abate, G., Massimino, M. (2016). Dynamic soil-structure interaction analysis by experimental and numerical modelling. *Riv Ital Geotec* 2/2016.
41. Régnier, J., Bonilla, L.-F., Bard, P.-Y., Bertrand, E., Hollender, F., Kawase, H., Sicilia, D., Arduino, P., Amorosi, A., Asimaki, D., Boldini, D., Chen, L., Chiaradonna, A., DeMartin, F., Elgamal, A., Falcone, G., Foerster, E., Foti, S., Garini, E., Gazetas, G., Gélis, C., Ghofrani, A., Giannakou, A., Gingery, J., Glinsky, N., Harmon, J., Hashash, Y., Iai, S., Kramer, S., Kontoe, S., Kristek, J., Lanzo, G., di Lernia, A., Lopez-Caballero, F., Marot, M., McAllister, G., Mercerat, E.D., Moczo, P., Montoya-Noguera, S., Musgrove, M., Nieto-Ferro, A., Pagliaroli, A., Passeri, F., Richterova, A., Sajana, S., Santisi d’Avila, M. P., Shi, J., Silvestri, F., Taiebat, M., Tropeano, G.,

Vandeputte, D.,Verrucci, L. (2018) PRENOLIN: International benchmark on 1D nonlinear site-response analysis -validation phase exercise. *B Seismol Soc Am* 108(2), 876-900.
42. Bilotta, E., Lanzano, G., Madabushi, S.P.G., Silvestri, F. (2014). A numerical Round Robin on tunnels under seismic actions. *Acta Geotech* 9:563-579. https://doi.org/10.1007/s11440-014-0330-3
43. Manzari, M. T., El Ghoraiby, M., Zeghal, M., Kutter, B. L., Arduino, P., Barrero, A. R., Bilotta, E., Chen, L., Chen, R., Chiaradonna, A., Elgamal, A., Fasano, G., Fukutake, K., Fuentes, W., Ghofrani, A., Haigh, S. K., Hung, W.-Y., Ichii, K., Kim, D. S., Kiriyama, T., Lascarro, C., Madabushi, G. S. P., Mercado, V., Montgomery, J., Okamura, M., Ozutsumi, O., Qiu, Z., Taiebat, M., Tobita, T., Travasarou, T., Tsiaousi, D., Ueda, K., Ugalde, J., Wada, T., Wang, R., Yang, M., Zhang, J.-M., Zhou, Y.-G., Ziotopoulou, K. (2019). LEAP-2017: Comparison of the Type-B Numerical Simulations with Centrifuge Test Results. *In: B. Kutter et al. (Eds.), Model tests and numerical simulations of liquefaction and lateral spreading: LEAP-UCD-2017*. New York: Springer.
44. Ghofrani, A., Arduino, P. (2018). Prediction of LEAP centrifuge test results using a pressure-dependent bounding surface constitutive model. *Soil Dyn and Earthq Eng* 113, 758-770. https://doi.org/10.1016/j.soildyn.2016.12.001
45. Gajo, A. (2010). Hyperelastic modelling of small-strain anisotropy of cyclically loaded sand. *Inter J Numer Anal* 34(2), 111-134. https://doi.org/10.1002/nag.793
46. Durante, M. G. (2015). Experimental and numerical assessment of dynamic soil-pile-structure interaction. *PhD Thesis*. Università degli Studi di Napoli Federico II.
47. Crewe, A., J., Lings, M., L., Taylor, C., A., Yeung, A., K., Andrighetto, R. (1995). Development of a large flexible shear stack for testing dry sand and simple direct foundations on a shaking table. European seismic design practice, Elnashai (ed), Balkema, Rotterdam.
48. Tan, F.S.C. (1990). Centrifuge and theoretical modelling of conical footings on sand. *PhD Thesis*. University of Cambridge.
49. Moccia, F. (2009). Seismic soil pile interaction: experimental evidence. *PhD Thesis*. Universita degli Studi di Napoli Federico II.
50. Kowalczyk, P. (2020). Validation and application of advanced soil constitutive models in numerical modelling of soil and soil-structure interaction under seismic loading. *PhD thesis*. University of Trento. http://hdl.handle.net/11572/275675
51. Dassault Systèmes (2019). Abaqus Standard software package.
52. Gajo, A. (2017). Fortran subroutine in a format of user defined material (UMAT) of the implementation of the Severn-Trent sand model.
53. Been, K., Jefferies, M., J. (1985). A state parameter for sands. *Géotechnique* 35, 99-112. https://doi.org/10.1680/geot.1985.35.2.99
54. Dietz, M., Muir Wood, D. (2007). Shaking table evaluation of dynamic soil properties. *In proceedings of: 4th International Conference of Earthquake Geotechnical Engineering*, June 25-28, Thessaloniki, Greece.
55. Seed, H. B., Idriss, I. M. (1970). Soil moduli and damping factors for dynamic response analysis. EERC report 70-10. University of California, Berkeley
56. Kokusho, T. (1980). Cyclic triaxial test of dynamic soil properties for wide strain range. *Soils Found* 20(2), 45-60. https://doi.org/10.3208/sandf1972.20.2_45
57. Shahnazari, H., Towhata, I. (2002). Torsion shear tests on cyclic stress-dilatancy relationship of sand. *Soils Found* 42(1) 105-119. https://doi.org/10.3208/sandf.42.105
58. Watanabe, K., Pisano, F., Jeremic, B. (2017). Discretization effects in the finite element simulation of seismic waves in elastic and elastic-plastic media. *Eng Comput* 33, 519-545. https://doi.org/10.1007/s00366-016-0488-4
59. Uesugi, M., Kishida, H. (1986). Influential factors of friction between steel and dry sands. *Soils Found* 26(2), 33-46. https://doi.org/10.3208/sandf1972.26.2_33
60. Kowalczyk, P., Gajo, A. (2022). Introductory consideration supporting the idea of the release of unloading elastic waves in the steady state response of hysteretic soil. (Under completion)
61. Kowalczyk, P. (2022). Resonance of a structure with soil elastic waves released in nonlinear hysteretic soil upon unloading. *Studia Geotechnica et Mechanica.* (In press)
62. Kuwano, R., Jardine, R.J. (2002). On the applicability of cross-anisotropic elasticity to granular materials at very small strains. *Géotechnique* 52:727-749. https://doi.org/10.1680/geot.2002.52.10.727